Underwater Acoustic Power Around Submerged Body in Shallow Water Using Boundary Element Method

M. Fatkhurrozi & Irsan S. Brodjonegoro*

Ocean Engineering Program, Faculty of Civil and Environmental Engineering, Institut Teknologi Bandung, Jalan Ganesha 10, Bandung 40132, Indonesia
*E-mail: irsansb@ocean.itb.ac.id

Abstract. Underwater acoustic power around a submerged body in shallow water was investigated using the Boundary Element Method (BEM). The model domain simulated a nearshore environment with shallow water conditions. The seabed was assumed flat and sound velocity was constant over depth. The boundary element method was combined with eigenfunction expansion to model radiation boundary conditions. Underwater acoustic power was calculated from the underwater acoustic potential in the domain. Several cases were investigated in this study: cases with variation of submerged body distance from the seabed, variation of submerged body location from the underwater acoustic source, and variation of submerged body length.

Keywords: *boundary element method; shallow water; submerged body; underwater acoustics; underwater acoustic power.*

1 Introduction

Early numerical methods for solving underwater acoustic problems, such as the parabolic equation, normal modes, and ray tracing, have several restrictions, as described by Jensen, *et al.* [1]. Parabolic equation methods neglect backscattering effects, which are likely to be important in shallow water and near the shoreline. These methods are used for shallow water propagation in horizontally stratified media. They are best suited for low-frequency problems but experience difficulties with a domain (the area where the computation is conducted) that is both range- and depth-dependent. Ray tracing deals with bottom interactions only in an approximate manner and therefore is not suitable to simulate shallow water.

Discretization-based methods e.g. the finite difference method (FDM) and the finite element method (FEM), have been developed to solve underwater acoustic problems with complex domain geometries. FDM places a grid of 'cells' inside the domain and applies the differencing approximation to each interior point. FEM divides the domain into small finite segments where their behavior is described by a suitable shape function. As its name implies, the discretization of the boundary element method (BEM) is only over the boundary

Received December 11th, 2017, 1st Revision August 7th, 2018, 2nd Revision March 19th, 2019, 3rd Revision June 11th, 2019, 4th Revision August 13th, 2019, Accepted for publication September 12th, 2019.
 ISSN: 2337-5779, DOI: 10.5614/j.eng.technol.sci.2019.51.5.9

of the domain, reducing the number of unknowns by one order. This method computes the internal point value by employing a boundary integral equation. Compared to BEM, FDM has difficulty fitting complex boundary geometries as it employs a rectangular grid to discretize the domain. FEM is less effective in computational aspects as the discretization is over the entire domain [2].

In this study, underwater acoustic propagation was modeled in shallow water representative of coastal regions, where sound velocity is constant over depth. The existence of a submerged body in the model escalates the geometry's complexity so the use of BEM is an appropriate solution. The submerged body was a cylindrical shell structure, which has been modeled in numerous previous papers due to its regularity [3]. This underwater acoustic wave modeling is used in active acoustic systems to detect the existence of submerged bodies (e.g. submarines) in water.

The underwater acoustic power was calculated from the underwater acoustic potential in the domain. The problems modeled in this study were: problems with variation of the submerged body's distance from the seabed, variation of the submerged body's location related to the underwater acoustic source, and variation of the submerged body's length.

2 Methodology

The boundary element computation conducted in this study used the 2D Boundary Element Method Helmholtz Solver (2DBEMHS) developed by Stéphan T. Grilli from the University of Rhode Island. The program inputs are wavenumber, node per-wavelength, domain geometry, submerged body geometry, source location, modes used in radiation boundary. The computation resulted in the underwater acoustic potential ($\emptyset$) in the boundary and the domain that was used to calculate the underwater acoustic power.

Validation was conducted on a problem with a rectangular boundary geometry of which the analytical solution was known. An error criterion of 5% was used in this validation. Once the model was validated, the underwater acoustic potential ($\emptyset$) in the boundary and the domain was calculated.

3 Mathematical Formulation

3.1 Boundary Integral Equation

The complex velocity potential for homogeneous harmonic two-dimensional problems in the vertical plane, (x, z), is [4]:

$$\Phi(\mathrm{x},\mathrm{z},\mathrm{t}) = \emptyset(\mathrm{x},\mathrm{z})e^{-i\omega t} \tag{1}$$

with velocity $\mathbf{u} = \nabla\Phi$, ω is the acoustic wave angular frequency, $\emptyset$ is the complex potential amplitude, and i is an imaginary number ($i = \sqrt{-1}$). Sound velocity c is assumed to be constant and ideal fluid theory is employed.

The governing Eq. (1) reduces to the following Helmholtz equation:

$$\nabla^2\emptyset + k^2\emptyset = 0 \tag{2}$$

where k is the wavenumber ($k = \omega/c$), and ∇ is the divergence operator.

The fundamental solution of Eq. (2) is

$$G = -\frac{\mathrm{i}}{4}H_0^{(2)}(kr) \tag{3}$$

The normal derivative of Eq. (3) is

$$\frac{\partial G}{\partial n} = \frac{ik}{4}H_1^{(2)}(kr)\frac{\partial r}{\partial n} \tag{4}$$

where r is distance between the source point and the field point, $H_0^{(2)}$ is a zero-order Hankel function of the second kind, $H_1^{(2)}$ is a first-order Hankel function of the second kind, and n is the unit normal vector.

The first step in the boundary element method is transforming governing Eq. (2) to a boundary integral equation, i.e. [2]

$$C^0(Q')\emptyset(Q') - \int_\Gamma G(Q',Q)\frac{\partial\emptyset(\mathrm{Q})}{\partial n}d\Gamma + \int_\Gamma \emptyset(\mathrm{Q})\frac{\partial \mathrm{G}(\mathrm{Q}',\mathrm{Q})}{\partial n}d\Gamma = 0 \tag{5}$$

where Q and Q' are the field point and source point respectively, $d\Gamma$ is a boundary segment, and C^0 is a coefficient depending on the boundary geometry (equal to ½ on a smooth boundary and 1 inside the domain).

For the case where sources exist, Eq. (5) becomes Eq. (6):

$$C^0(Q')\emptyset(Q') - \int_\Gamma G(Q',Q)\frac{\partial\emptyset(\mathrm{Q})}{\partial n}d\Gamma + \int_\Gamma \emptyset(\mathrm{Q})\frac{\partial \mathrm{G}(\mathrm{Q}',\mathrm{Q})}{\partial n}d\Gamma = \sum_{i=1}^{N_s} S_i G(Q',Q) \tag{6}$$

where the values S_i denote the strengths of N_s point sources located in the domain.

3.2 Boundary Conditions

The submerged body in shallow water is shown in Figure 1. The model is two-dimensional (x, z) and represents ocean sections near coastal regions with a sloping geometry and one open boundary on the offshore side.

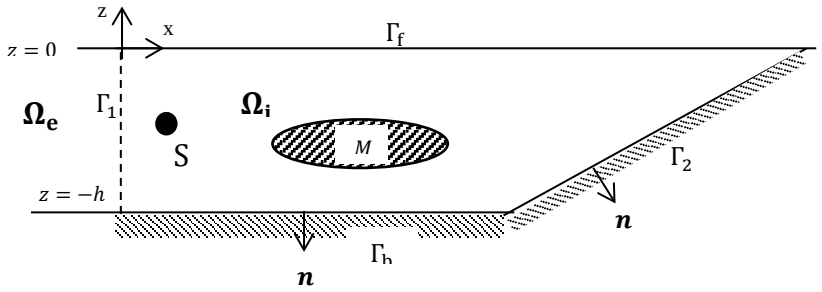

Figure 1 Shallow water region with submerged body model.

The depth of the water is h, and the submerged body is M. Ω_i is the domain where underwater acoustic potential is computed, while Ω_e is the offshore region where the potential is not computed, bounded by radiation boundary Γ_1. The underwater acoustic potential is discretized on the boundary and numerically computed under the excitation of underwater acoustic source S, which is located at (x_s, z_s).

The boundary conditions are described as follows:

The rigid sea bottom is represented by Γ_b and Γ_2. Sloping boundary (Γ_2) indicates that the model resembles a nearshore environment. No-flow condition is applied to both Γ_b and Γ_2, that is

$$\frac{\partial \bar{\emptyset}}{\partial n} = 0 \tag{7}$$

The surface of the submerged body also utilizes this no-flow condition. The overbar denotes a prescribed value. At surface boundary Γ_f, where atmospheric pressure $p = 0$, no-wave condition is represented by

$$\bar{\emptyset} = 0 \tag{8}$$

Boundary Γ_1 is called the radiation boundary condition, where the potential and its normal gradient are continuous from inside the computational domain to the outside,

$$\frac{\partial \emptyset^e}{\partial n} = \frac{\partial \emptyset^i}{\partial n} \text{ and } \emptyset^e = \emptyset^i \text{ on } \Gamma_1 \tag{9}$$

The potential on Γ_1 can be represented by eigenfunction expansion derived from the normal mode solution, which satisfies the governing equation and both bottom and free surface boundary conditions (Eqs. (8) and (9)) [6]:

$$\emptyset = \sum_{m=1}^{N_m} A_m \sin(k_m z)\, e^{i\sqrt{k^2-k_m^2}|x|} \tag{10}$$

where k_m is *eigenvalue* $[k_m = \pi(2m-1)/2h]$ for the mth mode, and N_m is the number of *modes* used ($N_m = 15$). Its normal gradient is in Eq. (11).

$$\frac{\partial \emptyset}{\partial n} = i \sum_{m=1}^{N_m} A_m \sqrt{k^2 - k_m^2} \sin(k_m z)\, e^{i\sqrt{k^2-k_m^2}|x|} \tag{11}$$

The orthogonality of the eigenfunctions is used to derive the equation relating the potential and its gradient:

$$\int_{-h}^{0} sin(k_l z)\, sin(k_m z)\, dz = \frac{h}{2}\delta_{lm} \tag{12}$$

The expansion coefficient is obtained from multiplying the potential in Eq. (7) by $\sin(k_l z)$ and integrating over depth in Eq. (13):

$$A_l = \frac{2}{h} e^{-i\sqrt{k^2-k_l^2}|x|} \int_{-h}^{0} \emptyset\ sin(k_l z)\, dz \tag{13}$$

Substituting this expansion coefficient into Eq. (8), for $l = m$, we get the relationship between the potential and its normal gradient along the radiation boundaries in Eq. (14):

$$\frac{\partial \emptyset}{\partial n} = \frac{2i}{h} \sum_{m=1}^{N_m} \sqrt{k^2 - k_m^2} \sin(k_m z) \int_{-h}^{0} \emptyset \sin(k_m z)\, dz \tag{14}$$

3.3 Discretization

To solve the boundary integral equation numerically, first the boundary must be discretized into a number of elements. The geometry (x, y) of each element can be represented by interpolation between the nodal points. They are in Eqs. (15) and (16)[4]:

$$x = \sum_{i=1}^{N_n} x_i\, N_i\, (\xi) \tag{15}$$

$$y = \sum_{i=1}^{N_n} y_i\, N_i\, (\xi) \tag{16}$$

where x_i and y_i are the coordinates at the nodal points, $N_i\,(\xi)$ is the shape function defined by local coordinate $-1 \le \xi \le 1$, and N_n is the number of nodes in the element. A quadratic element is employed in this discretization. Its shape functions are in Eqs. (17) to (19):

$$N_1 = -\frac{1}{2}\xi(1-\xi) \tag{17}$$

$$N_2 = (1-\xi^2) \tag{18}$$

$$N_3 = \frac{1}{2}\xi(1+\xi) \tag{19}$$

The boundary variables, $\emptyset$ and $\partial\emptyset/\partial n$, are represented by the same set of shape functions that are used to represent the geometry. They are:

$$\emptyset = \sum_{i=1}^{N_n} \emptyset_i \, N_i \, (\xi) \tag{20}$$

$$\frac{\partial \emptyset}{\partial n} = \sum_{i=1}^{N_n} \frac{\partial \emptyset_i}{\partial n} \, N_i \, (\xi) \tag{21}$$

Collocation is done by successively placing $\emptyset$ at each of the nodal points on the boundary. For each collocation point $\emptyset$, Eqs. (20) and (21) are subtituted into the boundary integral equation (Eq. (4)), integrating the equation over the boundary. The integration is done on an element-by-element basis. Each collocation point $\emptyset$ and element Γ_e combination produces two 'element coefficient vectors' in Eqs. (22) and (23):

$$h_e = \int_{\Gamma_e} \frac{\partial G}{\partial n} N_i \, d\Gamma \tag{22}$$

$$g_e = \int_{\Gamma_e} G N_i \, d\Gamma \tag{23}$$

Assembling h_e into global matrix $[H^*]$ and g_e into global matrix $[G]$, and applying to Eq. (6) produces Eq. (24).

$$[C]\{\emptyset\} + [H^*]\{\emptyset\} = [G]\left\{\frac{\partial \emptyset}{\partial n}\right\} \tag{24}$$

where [C] is a diagonal matrix consisting of geometry coefficient c. Combining $[C]$ and $[H^*]$ into one single matrix $[H]$ yields in Eq. (25).

$$[H]\{\emptyset\} = [G]\left\{\frac{\partial \emptyset}{\partial n}\right\} \tag{25}$$

Each component in $[H]$ and $[G]$ corresponds to unknown node values on the boundary ($\emptyset$ for [H]. Then $\frac{\partial \emptyset}{\partial n}$ for [G]) are arranged into a new matrix $[A]$ while the components corresponding to known values on the boudary are arranged into vector $\{b\}$. This produces a new system of equations:

$$[A]\{x\} = \{b\} \tag{26}$$

Eq. (26) can be solved by a standard matrix solver to get the unknown values on the boundary. Once the unknown values of $\emptyset$ and $\frac{\partial \emptyset}{\partial n}$ on the boundary have been solved, the $\emptyset$ in the domain can be obtained by solving Eq. (6) numerically.

3.4 Discretization of Underwater Acoustic Power

Once $\emptyset$ for the entire internal domain in a grid is known, the underwater acoustic power can be calculated by [5]

$$W = \frac{1}{2} Re \left[i\rho_0 \omega \int_{-h}^{0} \left\{ \emptyset \frac{\partial \phi^*}{\partial n} \right\} dz \right] \tag{27}$$

where ρ_0 is the water density, ω is the angular frequency, Re is the real part. The acoustic power, W, is determined by evaluating Eq. (27) over a vertical line in x.

4 Software Validation

2DBEMHS was validated for simple geometries of which the analytical solution is known. The case was selected from Grilli, *et al*. [5], which is a rectangular domain in two dimensions, as shown in Figure 2.

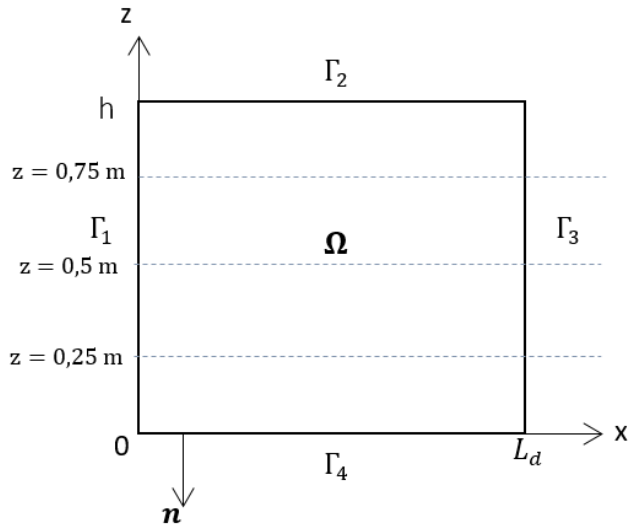

Figure 2 Simple case with rectangular domain.

The potential on boundary Γ_1 is specified with some value so as to easily derive an analytic solution. The boundary conditions thus read in Eq/ (28):

$$\emptyset(0, z) = -\frac{1}{\omega\rho_0} \cot(kL_d) \qquad \{x = 0; 0 \le z \le h\}$$

$$\frac{\partial \emptyset}{\partial n} = 0 \begin{Bmatrix} x = L_d; 0 \le z \le h \\ z = h; 0 \le x \le L_d \\ z = 0; 0 \le x \le L_d \end{Bmatrix} \tag{28}$$

where h is the domain height and L_d is the domain length. The analytic solution of $\emptyset$ (magnitude) to this problem is represented by Eq. (29).

$$\emptyset(x,z) = \left|\frac{1}{\omega\rho_0}\left\{\sin(kx) + \frac{\cos(kx)}{\tan(kL_d)}\right\}\right| \quad (29)$$

where $h = L_d = 1$, $\omega\rho_0 = 1{,}00$, and $kh = 8$.

Figure 3 shows a comparison between the analytical result and the numerical results for potential $\emptyset$. Three z coordinates (z =0.25 m, 0.5 m, and 0.75 m) were chosen to represent the numerical results. There are small inaccuracies in several points of x that will be discussed in the next paragraph.

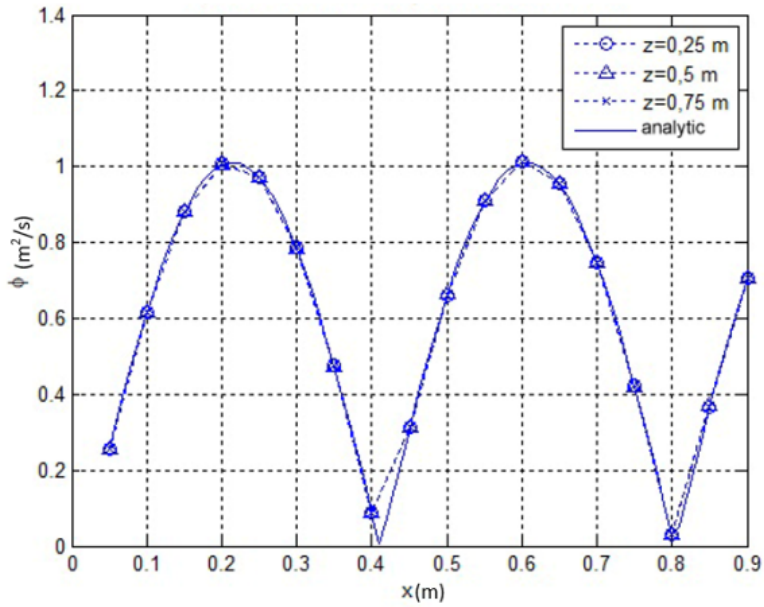

Figure 3 Potential result of the analytical and the numerical solution for three z coordinates (z = 0.25 m, 0.5 m, and 0.75 m) for a rectangular domain.

The error for each point of x is calculated by the following formula:

$$\varepsilon = \left|\frac{\emptyset_b - \emptyset_a}{\emptyset_a}\right| \times 100\% \quad (30)$$

where index a refers to the analytical solution and index b to the numerical solution. The error plot over the x axis for z = 0.25 m, 0.5 m, and 0.75 m is depicted in Figure 4. As can be seen in Figure 4, the numerical results have a maximum error of 2.5% (for z = 0.5 m) at x = 0.8 m. The average error over the entire domain is 0.465%. This means that there is overall agreement between the analytical and the numerical results. 2DBEMHS was then used to calculate a model with a more complex geometry.

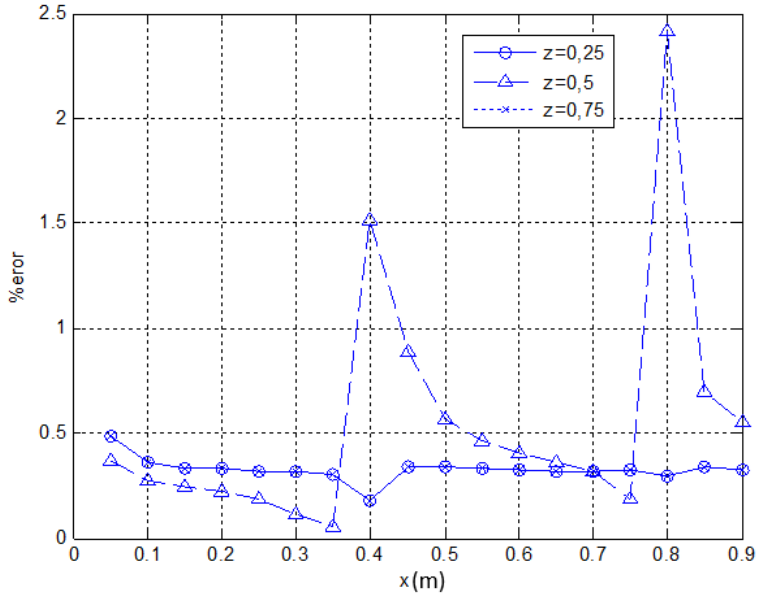

Figure 4 Error plot for the numerical solution for three z coordinates ($z = 0.25$ m, 0.5 m, and 0.75 m) for a rectangular domain.

5 Problem Modeling and Results

The validated 2DBEMHS was then used to model underwater acoustic propagation with a more irregular boundary geometry. This case represents a shallow water region near the coast with a submerged body inside the water, as shown in Figure 5. The case is scaled at 10:1. The density of the water is $\rho = 1025\ kg/m^3$, underwater sound speed is $c = 1500$ m/s, and wavenumber k = 3.55. The boundaries are numbered 1 to 4.

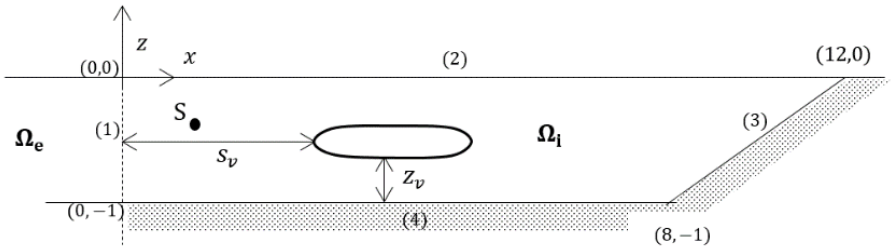

Figure 5 Shallow water region with submerged body used in this model.

z_v is the distance between the submerged body and the seabed, and s_v is the distance of the submerged body on the x axis. The source with strength $S = 1$ is located at $x_s = 1$ and $z_s = 0.5$. Sea bottom boundaries Γ_b and Γ_2 are rigid, therefore no-flow condition applies ($\partial\emptyset/\partial n = 0$). The surface of the submerged body also utilizes this no-flow condition. At surface boundary Γ_f, no-wave condition $\overline{\emptyset} = 0$ is present. Γ_1 is a lateral open boundary treated as radiation boundary condition. The submerged body dimensions are depicted in Figure 6.

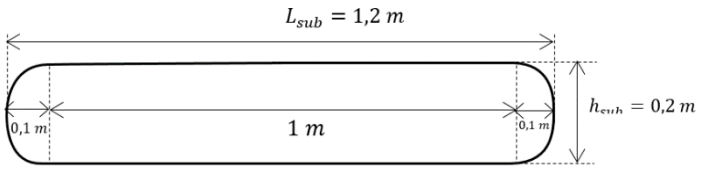

Figure 6 Submerged body dimensions used in the model.

The boundaries of the domain were discretized by 15 nodes per wavelength. As the elements employed were of a quadratic type, each of them contained 3 nodes. The number of elements on each of the boundaries was equal to $(N_o - 1)/2$, where N_o is the number of nodes of the corresponding boundary. As the domain was inside the boundaries, the entries for the coordinates of the boundary elements are read in counterclockwise order. The nodes and elements in all boundaries produce the scheme in Figure 7. For the submerged body, 13 nodes discretize its boundaries, so it contains 6 elements. For plotting the results in the domain, 118 x 18 internal points (horizontal x vertical) were employed.

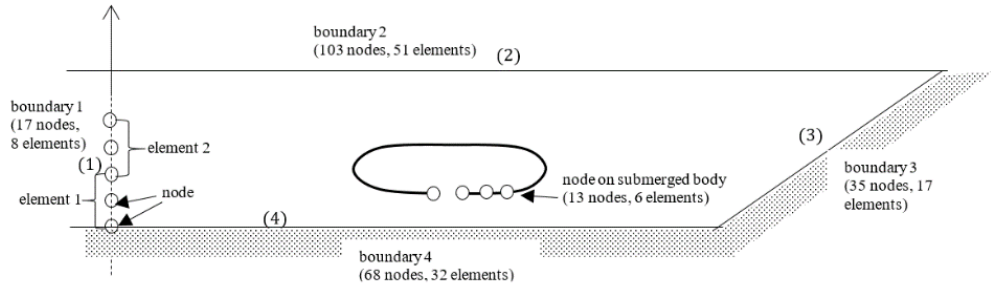

Figure 7 Illustration of discretization of the model.

5.1 Underwater Acoustic Potential

Figure 8 shows the potential field obtained by numerical computation. It can be seen that the potential in the surface region has zero value, representing a

pressure-release boundary condition. In the bottom, there is the periodic potential value resulted from the wave equation.

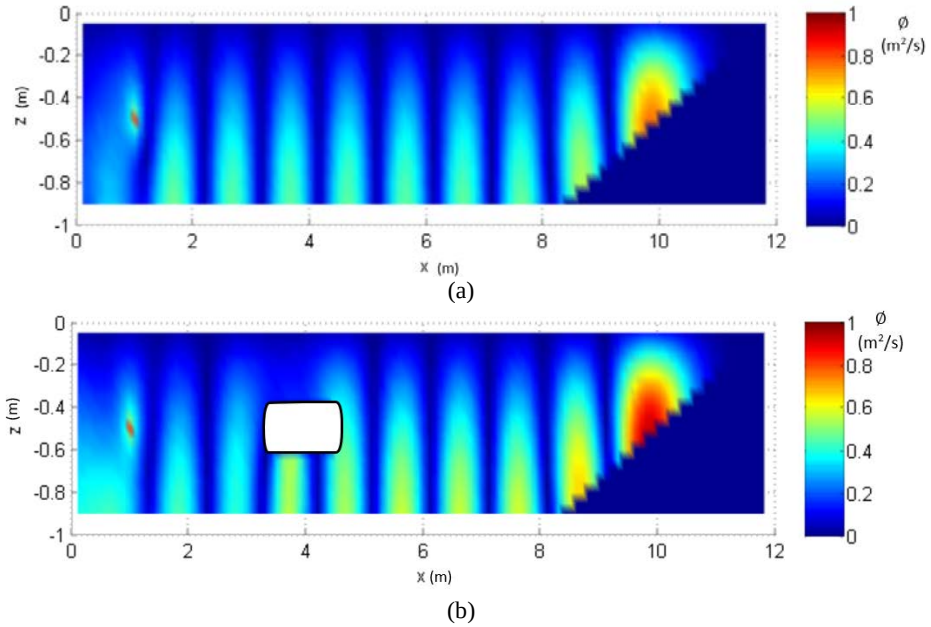

Figure 8 Plot of potential for a shallow water geometry (k = 3.55), (a) without submerged body, (b) with submerged body.

There is a potential increase over the slope ($8 < x < 12\,m$) with maximum value 0.75 m^2/s in Figure 8(a) and 0.91 m^2/s in Figure 8(b). At the offshore side ($1 < x < 8\,m$) the maximum potential is 0.56 m^2/s in Figure 8a and 0.69 m^2/s in Figure 8(b). The existence of a submerged body in the shallow water enhances the potential field in the domain.

The potential plot for the regions under the submerged body can be seen in Figure 9. This plot gives the details of the differences in potential resulted from the case in Figures 8(a) and (b) in the range of 3.1 m $< x <$ 4.7 m for z = -0.8 m. It indicates that there is an increase in average potential for the case with a submerged body. From the calculation, the increment is 15%. This is caused by the existence of the submerged body, which enhances the potential in the region where the submerged body resides.

5.2 Underwater Acoustic Power

Underwater acoustic power, W, was then calculated using Eq. (21) for $1.1\ m < x < 11.7\ m$, as depicted in Figure 10.

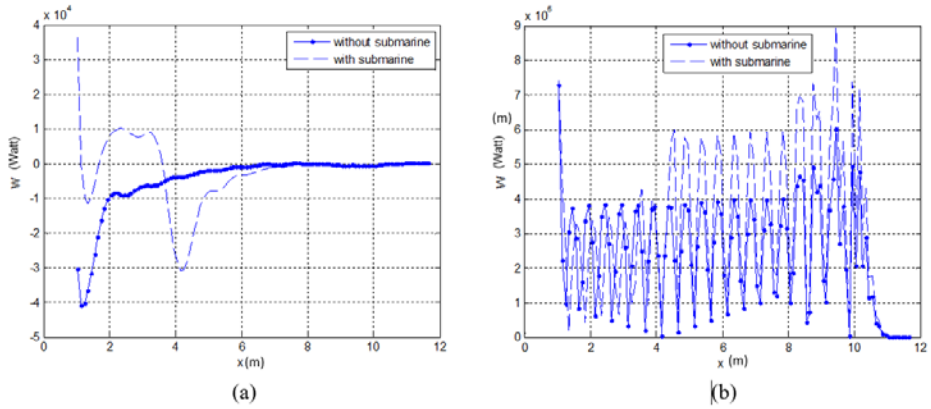

Figure 9 Plot of underwater acoustic power W (k = 3,55). The submerged body is located at $x = 3.37$ m to $x = 4.57$ m, (a) real value, and (b) magnitude.

As can be seen in Figure 10a, there is significant difference in the real value of underwater acoustic power between both cases for $1.1\ m < x < 7\ m$. In the case with submerged body, there is a positive value at about 1 x 10^4 watt within that range while in the case without submerged body it is negative over the entire x axis. At $3.3\ m < x < 4.15\ m$, the real value of the case with submerged body harshly drops $3 \cdot 10^4$ watt before increasing at x = 4.25 m.

As for the underwater acoustic power magnitude, Figure 10b shows that the case with submerged body has a larger result over the x axis than the case without submerged body, except at $1.8\ m < x < 3.6\ m$, where both cases seem to have the same value. Calculation of the average value shows that the case in which submerged body is located in the domain has an average magnitude of underwater acoustic power 1.33 times greater than the case without submerged body. This is evidence that the existence of a submerged body in the domain enhances the magnitude of the underwater acoustic power.

5.3 Variation of Submerged Body Distance from Seabed

The next calculation was conducted on the cases with variation of the distance of the submerged body from the seabed, z_v (Figure 5). The five z_vs used in the model were: $z_v = 0.2$ m, $z_v = 0.3$ m, $z_v = 0.4$ m, $z_v = 0.5$ m, and $z_v = 0.6$ m. The same values of ρ, c, and k were used in this case. The results are shown in Figure 11.

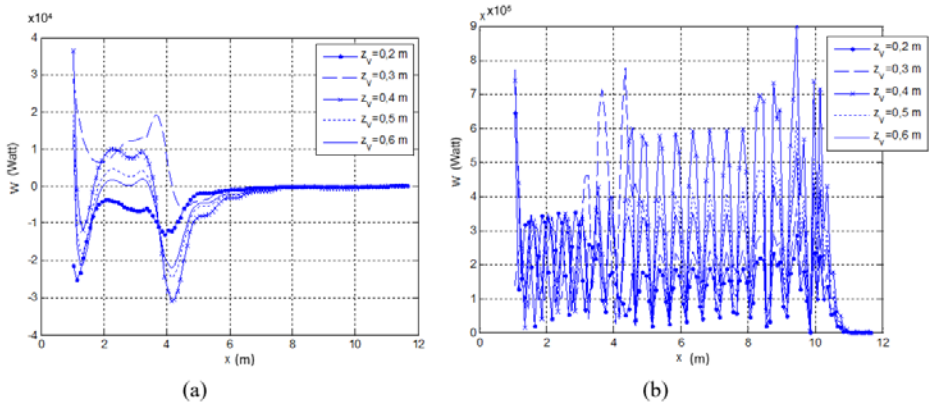

Figure 10 Plot of underwater acoustic power with various submerged body distance from seabed, z_v, (a) real value, and (b) magnitude.

Figure 11(a) shows that the real value of underwater acoustic power shared the same behavior in all cases, except for the case with $z_v = 0.3$ m. The value of the case with $z_v = 0.3$ surges from $x = 2$ m to $x = 3.8$ m, while the others go down. Entering the submerged body area ($x = 3.3$ m), the real W values of all cases decrease. The sharp drop occured in the cases with $z_v = 0.3\,m$. The case with $z_v = 0.3\,m$ has a positive value of real acoustic power over the other cases.

As can be seen in Figure 11(b), the underwater acoustics power magnitude has the same periodic behavior for all cases at 4.4 m $< x <$ 11 m. The maximum and minimum average value of underwater acoustic power magnitude for all cases occurs at $x = 9.4$ m and $x = 0.2$ m respectively. The average underwater acoustic magnitude in the case with submerged body distance from the seabed $z_v = 0.4$ m is 2.2 times larger than the case with $z_v = 0.2$ m. In the offshore area (1 m $< x <$ 8 m), the minimum magnitude underwater acoustic power W occurs at x =1.35 m for the case with $z_v = 0.4$, where its value is 0.042 times below its average magnitude.

5.4 Variation of Submerged Body Location on *x* Axis

The next calculation was conducted on the cases with variation of submerged body distance in on the x axis, s_v (Figure 5). The five locations used in the model were: $s_v = 3.3\,m$, $s_v = 3.8\,m$, $s_v = 4.3\,m$, $s_v = 5.3\,m$, and $s_v = 7.8\,m$. The same values of ρ, c, and k were used in this case. The results are shown in Figure 12.

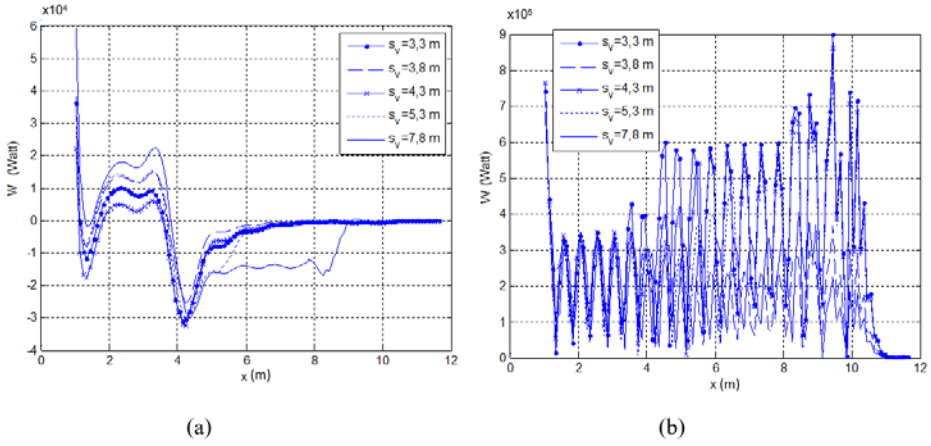

Figure 11 Plot of underwater acoustic power in the cases with various submerged body distances on the x axis s_v, (a) real value, and (b) magnitude.

Figure 12(a) shows that the real value of the underwater acoustic power for all cases has the same behavior in all cases at 1.1 m $< x <$ 4.5 m. The real value of the acoustic power in the case with $s_v = 7.8$ m is larger compared to the other cases while for the case with $s_v = 4.3$ m it is smaller. For $x >$ 4.5 m, the real value of the acoustic power in the case with $s_v = 3.8$ m is larger compared to the other cases. For 4.8 m $< x <$ 8.6 m, there is a relatively small value of the acoustic power for the cases with $s_v = 7.8$ m.

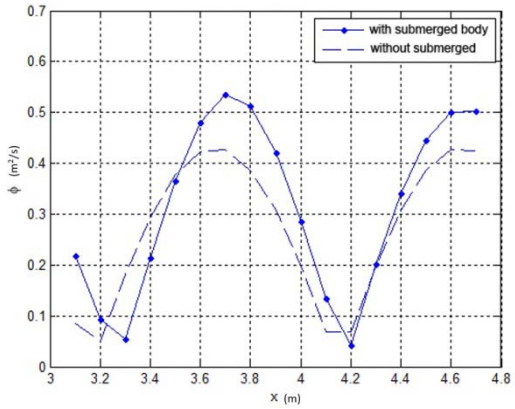

Figure 12 Potential plot for 3.1 $m <$ $x <$ 4.7 m for $z = -0{,}8\ m$.

As can be seen in Figure 12(b), there is apparently a different behavior of the acoustic power magnitude in all cases. In the case with submerged body distance on the x axis, s_v, s_v = 3.3 m, $s_v = 4.3$ m, and $s_v = 5.3$ m, there is a

relative increase of magnitude acoustic power in the area where the submerged body resides ($x = 4.4$ m). The cases with s_v = 3.8 m and $s_v = 7.8$ decrease at $x = 4.4$ m. The largest and the smallest average magnitude acoustic power occurs in the case with s_v =3.3 m and s_v =3.8 respectively. The case with s_v =3.3 m has a magnitude acoustic power that is 1.8 times larger than in the case with $s_v = 3.8$ m. In the offshore area ($1 \text{ m} < x < 8$ m), the minimum acoustic power magnitude occurs at $x = 0.45$ m in the case with $s_v = 2.3$ m, where its value is 0.042 times below its average magnitude.

5.5 Variation of Submerged Body Length

The next calculation was conducted on the cases with variation of submerged body length, L_{sub} (Figure 5). The five lengths of the submerged body used in the model were: $L_{sub} = 1.2\ m$, $L_{sub} = 1.21\ m$, $L_{sub} = 1.44\ m$, $L_{sub} = 1.8\ m$, and $L_{sub} = 2.4\ m$. The same values of ρ, c, and k are used in this case. The results are shown in Figure 13.

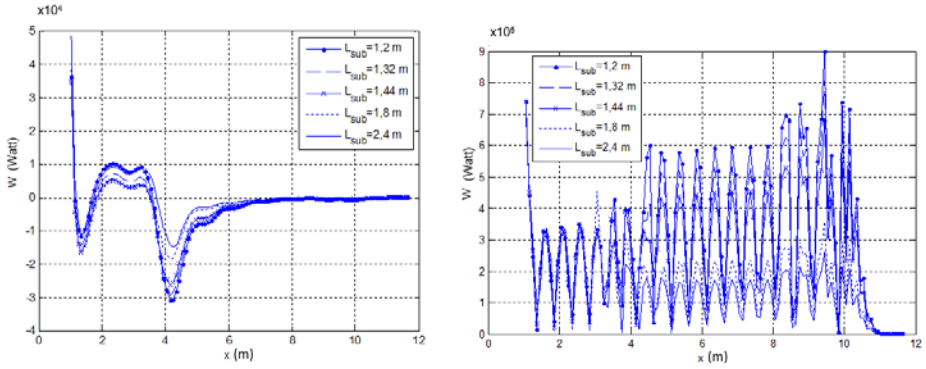

Figure 13 Plot of underwater acoustic power in the cases with various submerged body lengths, L_{sub}, (a) real value and (b) magnitude.

Figure 13(a) shows that the real value of the underwater acoustic power has the same behavior in all cases. There is a significant drop for all cases at $3.1 < x <$ 4.4 m. The case with submerged body length $L_{sub} = 1.2$ m has a relatively large value of real acoustic power at $2 < x < 3.5$ m and a relatively large negative value of real acoustic power at $3.5 < x < 4.4$ m.

As can be seen in Figure 13(b), the magnitude of acoustic power has the same behavior over the x axis in all cases, except at $x > 8$ m. The largest magnitude occurs at x = 9.4 m in all cases. The case with submerged body length $L_{sub} =$

1.2 m has a larger magnitude than the other cases, while the case with $L_{sub} =$ 2.4 m has a smaller magnitude than the other cases. The calculation indicates that the average magnitude of acoustic power for the case with submerged body length $L_{sub} =$ 2.4 m is 0.44 times smaller than the average magnitude of acoustic power in the case with L_{sub} = 1.2 m. This implies that the longer the submerged body, the smaller the average magnitude. In the offshore area ($1 \text{ m} < x < 8$ m), the minimum magnitude of acoustic power occurs at $x =$5.15 m in the case with $L_{sub} =$ 2.4 m, where its value is 0.024 times smaller than its average magnitude.

6 Conclusion

Numerical computation with the boundary element method was conducted on a shallow water problem with various submerged body locations and geometries. The existence of a submerged body in the domain enhances the underwater acoustic potential. The cases in which the submerged body is located within the domain has an average magnitude of underwater acoustic power (W) 1.33 times greater than the cases without submerged body.

In the cases where the distance of submerge body from the seabed (z_v) was varied, the greatest average and the lowest acoustic power occurred for a distance of $z_v = 0.4$ m and $z_v = 0.2$ m respectively. In the offshore area ($1 \text{ m} < x < 8$ m), the minimum magnitude of acoustic power occurs at $x =$ 1.35 m for case with $z_v = 0.4$, where its value is 0.042 times smaller than its average magnitude.

In the case with variation of distance from the source (s_v), the results show that the case with $s_v =$ 3.3 m has the greatest average acoustic power over the x axis and the case with $s_v =$ 3.8 m has smallest average acoustic power over the x axis. In the offshore area ($1 \text{ m} < x < 8$ m), the minimum magnitude of acoustic power occurs at $x =$0.45 m in the case with $s_v =$ 2.3 m, where its value is 0.042 times smaller than its average magnitude.

In the case with variation of submerged body length (L_{sub}), the results show that the case with L_{sub} = 1.2 m has the greatest average acoustic power over the x axis and the case with L_{sub}= 2.4 m has the smallest average W. In the offshore area ($1 \text{ m} < x < 8$ m), the minimum magnitude of acoustic power occurs at $x =$ 5.15 m for the case with $L_{sub} =$ 2.4 m, where its value is 0.024 times smaller than its average magnitude.

References

[1] Jensen F.B., Kuperman, W.A., Porter, M.B. & Schmidt, H., *Computational Ocean Acoustics*, 2nd ed., Springer, 531, 2011.

[2] Katsikadelis, J.T., *Boundary Elements Theory and Applications*, Elsevier, pp. 2-3, 2002.

[3] Jiang, L., Zou, M., Huang, H. & Feng, X., *Integrated Calculation Method of Acoustic Radiation and Propagation for Floating Bodies in Shallow Water*, The Journal of the Acoustical Society of America, **143**, pp. 431-436, 2018.

[4] Wu, T.W., *Boundary Element Acoustics: Fundamentals and Computer Codes*, WIT Press, Southhampton, UK, pp. 4-34, 2000.

[5] Grilli, S.T., Pedersen, T. & Stephanishen, P., *A Hybrid Boundary Element Method for Shallow Water Acoustic Propagation Over an Irregular Bottom*, Engineering Analysis with Boundary Elements, **21**, pp. 131-145, 1998.

[6] Grilli, S.T. & Skourup, J., *An Efficient Boundary Method for Nonlinear Water Wave*s, Engineering Analysis with Boundary Elements, **6**, pp. 97-107, 1989.

[7] Boas, M.L., *Mathematical Methods in The Physical Science*s, John Wiley and Sons Inc., pp. 274-275, 1966.

[8] Grilli, S.T. & Svendsen, I.A., *Corner Problems and Global Accuracy in The Boundary Element Solution of Nonlinear Wave Flows*, Engineering Analysis with Boundary Elements, **7**, pp. 178-195, 1990.

[9] Kinsler, L.E., Frey, A.R., Coppens, A.B. & Sanders, J.V., F*undamentals of Acoustics*. 3rd ed., John Wiley and Sons, pp. 99-107, 1982.

[10] Santiago, J.A.F. & Wrobel, L.C., *Numerical Modelling of the Propagation of Underwater Acoustic Waves*, 15th Brazilian Congress of Mechanical Engineering, 1999.